Available online at www.sciencedirect.com
SCIENCE DIRECT®
Journal of Nuclear Materials 329–333 (2004) 283–288
journal of nuclear materials
www.elsevier.com/locate/jnucmat

Microstructure property analysis of HFIR-irradiated reduced-activation ferritic/martensitic steels

H. Tanigawa [a,*], N. Hashimoto [b], H. Sakasegawa [c], R.L. Klueh [b], M.A. Sokolov [b], K. Shiba [a], S. Jitsukawa [a], A. Kohyama [c]

[a] *Japan Atomic Energy Research Institute, 2-4 Shirakata, Tokai-Mura, Ibaraki-ken 319-1195, Japan*
[b] *Oak Ridge National Laboratory, Oak Ridge, TN 37831, USA*
[c] *Institute of Advanced Energy, Kyoto University, Uji, Kyoto 611-0011, Japan*

Abstract

The effects of irradiation on the Charpy impact properties of reduced-activation ferritic/martensitic steels were investigated on a microstructural basis. It was previously reported that the ductile–brittle transition temperature (DBTT) of F82H-IEA and its heat treatment variant increased by about 130 K after irradiation at 573 K up to 5 dpa. Moreover, the shifts in ORNL9Cr–2WVTa and JLF-1 steels were much smaller, and the differences could not be interpreted as an effect of irradiation hardening. The precipitation behavior of the irradiated steels was examined by weight analysis and X-ray diffraction analysis on extraction residues, and SEM/EDS analysis was performed on extraction replica samples and fracture surfaces. These analyses suggested that the difference in the extent of DBTT shift could be explained by (1) smaller irradiation hardening at low test temperatures caused by irradiation-induced lath structure recovery (in JLF-1), and (2) the fracture stress increase caused by the irradiation-induced over-solution of Ta (in ORNL9Cr–2WVTa).

1. Introduction

Reduced-activation ferritic/martensitic steels (RAF) are the most promising structural materials for fusion power plant reactors [1]. They are being investigated by the Japan Atomic Energy Research Institute (JAERI) and the Department of Energy (DOE), USA, in a collaboration program with emphasis on F82H (Fe–8Cr–2W–VTa), developed by JAERI and NKK Corporation [2]. Confidence in use of RAFs for early fusion power plants requires that the materials maintain their dimensional stability, strength, and adequate fracture toughness for the proposed application temperatures and fluence.

In a previous study [3], it was reported that ORNL9Cr–2WVTa and JLF-1 (Fe-9Cr–2W–V–Ta–N) steels undergo smaller ductile–brittle transition temperature (DBTT) shifts than IEA modified F82H (Fe–8Cr–2W–V–Ta) in its standard and alternate heat treatment conditions after neutron irradiation up to 5 dpa at 573 K. This difference in DBTT shift (ΔDBTT) was not correlated with the irradiation hardening, nor was it believed to be due simply to the difference in Cr concentration. Extensive microstructural analyses were performed to clarify the mechanisms of the difference in Charpy impact properties between these steels and the relation with tensile properties.

2. Experimental

The material used was IEA-modified F82H (F82H-IEA). Base metal with two heat treatment variations (standard IEA heat treatment and a heat treatment

* Corresponding author. Tel.: +81-29 282 6146/5391; fax: +81-29 282 5551/5922.
E-mail address: tanigawa@popsvr.tokai.jaeri.go.jp (H. Tanigawa).

0022-3115/$ - see front matter © 2004 Elsevier B.V. All rights reserved.
doi:10.1016/j.jnucmat.2004.04.053

Table 1
Chemical compositions of RAFs (wt%)

	C	Cr	W	V	Si	Ta	Ti	N
F82H-IEA	0.11	7.7	2.00	0.16	0.11	0.02	0.01	0.008
JLF-1	0.1	8.9	1.95	0.20	0.05	0.09	0.002	0.023
ORNL9Cr	0.1	8.8	1.97	0.18	0.21	0.07	<0.01	0.023

Table 2
Heat treatment conditions

F82H-IEA	1313 K/40 min/AC + 1023 K/1 h
F82H HT2	F 82H-IEA + 1193 K/1 h/AC + 1023 K/1 h
JLF-1	1323 K/1 h/AC + 1053 K/1 h
ORNL9Cr	1323 K/1 h/AC + 1023 K/1 h

designated HT2) was irradiated. ORNL9Cr–2WVTa (ORNL9Cr) and JLF-1 HFIR heat (JLF-1) were also irradiated for comparison. Details of the chemical compositions and the heat treatments are listed in Tables 1 and 2. Irradiation was performed in the ORNL HFIR Reactor to 5 dpa at 573 K in the removable beryllium (RB) position. Specimens selected for microstructure analyses were the 1/3 size Charpy specimens that fractured in a brittle mode (less than 1.0 J) on the lower shelf near the DBTT.

Vickers hardness tests (1 kgf) were carried out on both tensile specimens and Charpy impact specimens to make sure that the hardening levels are the same in both specimen types. Tensile tests were performed at 173 K on SS-3 tensile specimens with strain rate 1.0×10^{-3}/s to obtain yield stress change at low temperatures.

Extraction residues were obtained using a coarse filter (pore size 1 μm) and a fine filter (pore size 200 nm). XRD analyses were performed on residue samples. Extraction replica samples were prepared for unirradiated (normalized and tempered) materials. Details of these experiments are explained elsewhere [4,5]. TEM and X-ray energy-dispersive spectrometry (XEDS) analyses were performed on replica samples, and the fracture surfaces of Charpy impact-tested specimens were observed with SEM.

3. Results

Vickers hardness obtained from irradiated tensile and Charpy specimens were quite similar, as shown in Table 3. The results confirm that both types of specimen were irradiated in a practically identical condition.

Yield stresses (σ_y) at 173 K are shown in Table 4 with previously reported values included [3,6]. Note that the increase of σ_y was relatively small in JLF-1. Fracture stresses (σ_f) were estimated by assuming that σ_f is equal to three times σ_y at DBTT, which was extrapolated from

Table 3
Hardness and its standard deviation of irradiated tensile and CVN specimens

Hv(1 kgf)/(s.d.)	CVN	Tensile
F82H-IEA	288/(7)	286/(30)
F82H HT2	264/(10)	270/(10)
JLF-1	289/(10)	301/(13)
ORNL9Cr	312/(6)	339/(9)

measured σ_y because it is usually assumed that fracture initiation occurs at the most constrained region ahead of the initial crack under plain strain conditions. Note that σ_f of F82H-IEA, F82H HT2 and JLF-1 are about the same, but σ_f and $\Delta\sigma_f$ of ORNL9Cr are larger than for the other steels.

TEM observations on replica samples revealed that the majority of precipitates in F82H-IEA and HT2 were $M_{23}C_6$ with round and bulky shape; larger $M_{23}C_6$ precipitates were observed on prior austenite grain (PAG) and packet boundaries. Average diameters of these were 103 nm and 106 nm for F82H-IEA and HT2, respectively. On the other hand, $M_{23}C_6$ in JLF-1 and ORNL9Cr have a needle-like shape, and relatively large and bulky shaped $M_{23}C_6$ were observed on PAG, packet and lath boundaries. Average minor axis sizes of these were 121 and 111 nm for JLF-1 and ORNL9Cr, respectively. SEM back scattered electron (BSE) images and XEDS analysis confirmed the presence of round-shaped Ta-rich precipitates (MX) in the matrix of all steels. The size distribution and number density of MX are shown in Fig. 1(a). MX in F82H-IEA and HT2 were large and very few in number, but many fine MX particles were observed in JLF-1 and ORNL9Cr. It should be noted that MX particles in F82H-IEA and F82H HT2 contained a relatively large amount of Ti (Fig. 1(b)) compared to those in JLF-1 and ORNL9Cr (Fig. 1(c)).

SEM images of fracture initiation points are shown in Fig. 2. The initiation point was located by following the river patterns. Note that fractured precipitates or triple grain boundaries were observed as the fracture initiation points of each steel.

The mass of extracted residues before and after irradiation is shown in Fig. 3. Here the mass of residue obtained with the coarse filter (column denoted 'Large') is interpreted as the value corresponding to the mass of large precipitates, and the difference of mass obtained

Table 4
Yield stress (σ_y) at 173 K and at RT [3], DBTT [3] and estimated fracture stress (σ_f) of unirradiated and irradiated specimen of each RAF

(Unirrad./Irrad.)	σ_y at 173 K (MPa)	σ_y at 300 K (MPa)	DBTT (K)	Estimated σ_f (GPa)
F82H-IEA	571[a]/1002[a]	528/898	189/296	1.7/2.7
F82H HT2	598[a]/1026	501/865	172/276	1.8/2.7
JLF-1	641/942	525/839	188/236	1.9/2.7
ORNL9Cr	706/1229	577/1040	179/242	2.1/3.4

Here σ_f is assumed to be three times the value of σ_y at DBTT.
[a] Strain rate of these values are 1×10^{-4} (1/s) [6].

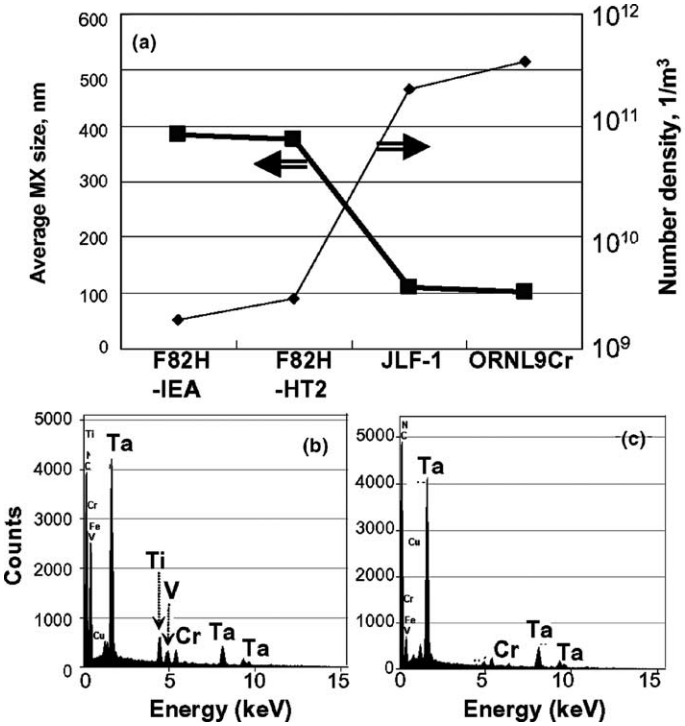

Fig. 1. (a) Number density and average size of MX (TaC) precipitates in each RAF, (b) typical EDX peaks obtained from MX precipitates in F82H-IEA and F82H HT2 and (c) those from JLF-1 and ORNL9Cr.

with the fine filter and the coarse filter (column denoted 'Small') is interpreted as that of the fine precipitates. These results indicate that during irradiation (1) the mass of larger precipitates increased in F82H-IEA, JLF-1 and ORNL9Cr, (2) no mass change occurred in F82H HT2 and (3) small precipitates disappeared in JLF-1.

The XRD analysis on extracted residue (Fig. 4) revealed that the majority of precipitates are $M_{23}C_6$ type (denoted with diamond mark) for all unirradiated and irradiated steels. The three distinctive peaks (denoted with triangle) are observed on unirradiated JLF-1 and ORNL9Cr, and those peaks are not detected on irradiated specimens. There is no exact match pattern for those peaks, but the best match is for the TaC peaks. This supposition is quite reasonable as the high number density of Ta-rich precipitates is observed in these steels (Fig. 1). The reason for these peak offsets would be that TaC is usually present as MX precipitate (M: Ta, V, Ti; X: C, N), as shown in Fig. 1(c).

4. Discussion

These results suggest that the large ΔDBTT of F82H-IEA and F82H HT2 were the results of the typical irradiation effects, i.e., the irradiation induced the hardening by the evolution of dislocation and precipitate structures,

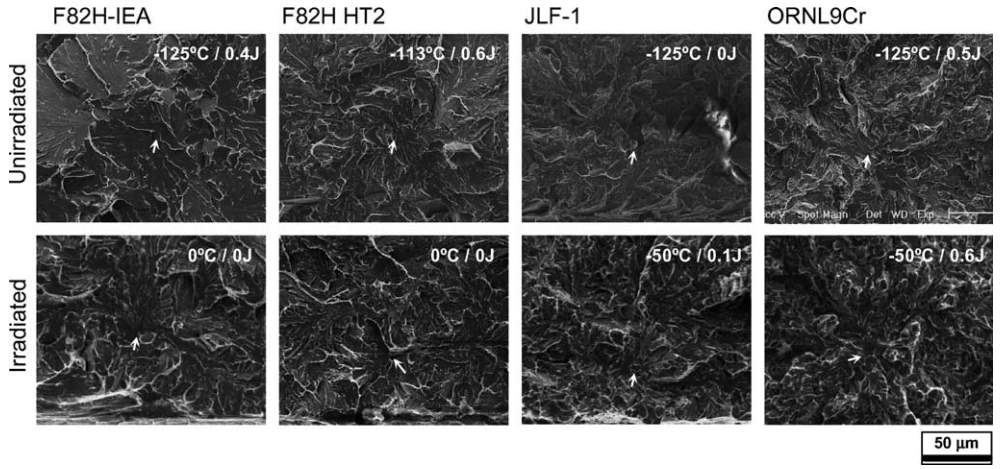

Fig. 2. SEM images of fracture initiation points on fractured CVN specimens of unirradiated and irradiated RAFs. Numbers in upper right of the images indicate test temperature and absorbed energy. White arrows indicate the precipitates observed on the surfaces. Crack propagated from bottom to top.

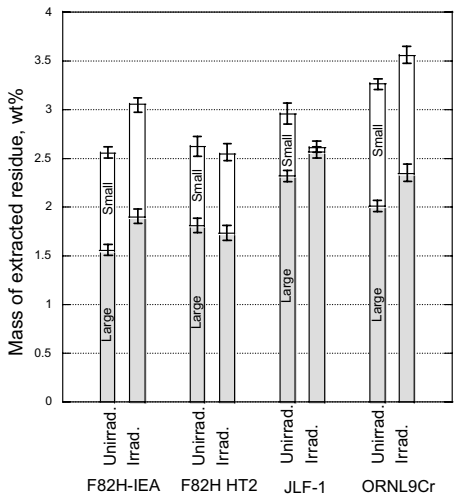

Fig. 3. Mass of extracted residue of unirradiated and irradiated RAFs extracted with coarse filter (Large) and fine filter (Large + Small).

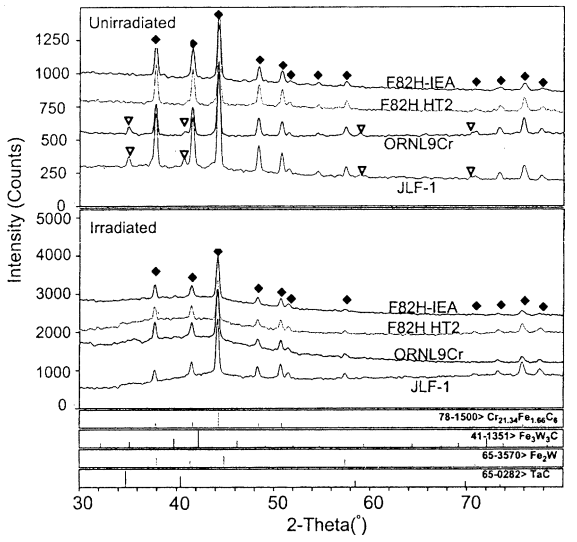

Fig. 4. XRD peaks of extracted residue from unirradiated and irradiated RAFs. Peaks marked with diamonds correspond to the peaks from $M_{23}C_6$, and with triangles correspond to that from MX (TaC).

and the irradiation hardening caused ΔDBTT. Here the smaller ΔDBTT of JLF-1 and ORNL9Cr are discussed.

Smaller ΔDBTT of JLF-1 can be simply explained by the small $\Delta\sigma_y$ at low temperature after irradiation. The reason for this could be explained by the possible lath structure recovery in JLF-1 under irradiation, because small precipitates in JLF-1 disappeared after irradiation, as shown in Fig. 3, and this tendency was also confirmed by TEM observations in another study [7]. This recovery of lath structure on JLF-1 was also reported previously for high-flux neutron irradiation [8], and in ion irradiation [9] at a relatively lower irradiation temperature compared to other RAFs.

On the other hand, the smaller ΔDBTT of ORNL9Cr in spite of a large $\Delta\sigma_y$ can be explained by the large $\Delta\sigma_f$. Irradiation effects on σ_f could be the result of a large increase of surface energy as follow. Here we assume that the critical cleavage fracture process in irradiated materials is the microcrack initiation ahead of a fractured precipitate on PAG or packet boundaries [10]. We postulate that fracture of a precipitate can be sponta-

neously induced by a dislocation pile up, as we observed fractured precipitates or grain boundary triple points on all crack-initiation sites (Fig. 2). If we assume the particle is spherical and a penny-shaped crack was induced across the diameter by dislocation pile up, then σ_f after irradiation ($\sigma_f^{irrad.}$) could be expressed by modifying equations in Ref. [10] as

$$\sigma_f^{irrad.} = \sqrt{\frac{\pi E((\gamma_s + \Delta\gamma_s) + (\gamma_p + \Delta\gamma_p))}{(1-\nu^2)(C_0 + \Delta C_0)}}, \quad (1)$$

where E is elastic modulus; ν is Poisson's ratio; C_0 is the average diameter or the average minor axis size of precipitates on PAG and packet boundaries; γ_s is the surface energy; and γ_p is the plastic work required to create a unit area of fracture surface. σ_f before irradiation ($\sigma_f^{unirrad.}$) can be expressed by making $\Delta\gamma_s$, $\Delta\gamma_p$, $\Delta C_0 = 0$. ΔC_0 could be estimated from the mass increase of large precipitates shown in Fig. 3 by assuming that the mass increase ratio is linearly correlated to the volume increase ratio, i.e., $((C_0 + \Delta C_0)/C_0)^3$, of precipitates on PAG and packet boundary. This assumption is reasonable as most large precipitates were observed on those boundaries. Based on these assumptions, γ_s, γ_p, $\Delta\gamma_s$, $\Delta\gamma_p$ are calculated (Table 5) from the estimated σ_f shown in Table 4. Here we may assume that $\gamma_p + \Delta\gamma_p$ is about the same for all RAFs, since it was reported that the dislocation microstructure of these RAFs did not show significant difference after irradiation [7]. Then the difference of $\Delta\gamma_s + \Delta\gamma_p$ for ORNL9Cr against other RAFs can be interpreted as the result of a large increase of surface energy ($\Delta\gamma_s$).

The possibility of large $\Delta\gamma_s$ was previously indicated as the cause for the DBTT difference between 9Cr–2WVTa and 9Cr–2WV steels [11]. It was suggested that the solute Ta increases surface energy and that caused the increase of fracture stress and a low DBTT. In this study, the XRD results (Fig. 4) suggest the possibility of TaC (MX) dissolution after irradiation of JLF-1 and ORNL9Cr. This phenomenon was also observed in an Fe–0.2Ta–0.015C alloy after ion irradiation, as shown in Fig. 5 [12]. Based on these results, we could assume that Ta returned to solution and increased the fracture stress of irradiated JLF-1 and ORNL9Cr.

The reason that this Ta effect did not appear in F82H, which also includes Ta, is due to the low Ta concentration and the relatively high Ti concentration in F82H. It is hypothesized that Ta in F82H is trapped on TiN and could not be dissolved, because Ti was included in TaC in F82H, as shown in Fig. 1, and Ti is known to act as a strong N getter and form stable TiN at high temperatures, and TaC is reported to nucleate around TiN [13]. This explanation also is applicable to explain the improved toughness of MOD3, the low Ti and N version of F82H, reported in this proceedings [14].

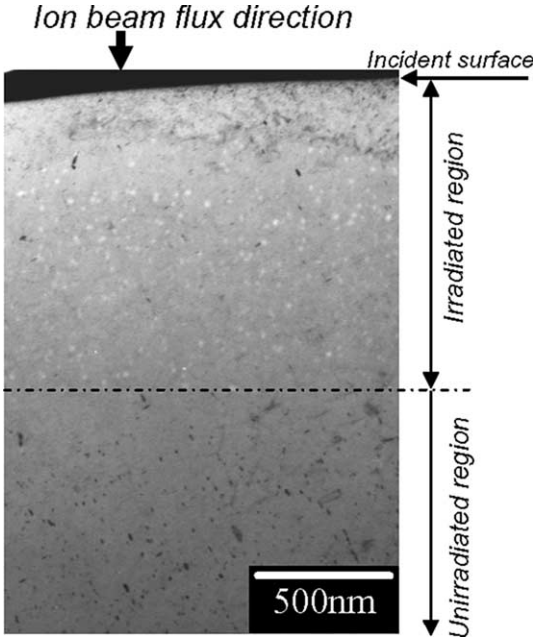

Fig. 5. Cross-sectional TEM bright field image of Fe–0.2Ta–0.015C alloy irradiated by 3.8 MeVFe^{3+} ion at 773 K up to 20 dpa (at 600 nm from incident surface) [12]. Black contrasts in not-irradiated region correspond to TaC.

5. Summary and conclusions

Reduced-activation ferritic/martensitic steels (RAFs) are being investigated in the JAERI/DOE collaboration program with the emphasis on F82H (Fe–8Cr–2W–VTa) to validate the potential of RAFs as structural materials for fusion power plants. The mechanisms for the difference in DBTT shift observed on four RAFs after irradiation up to 5 dpa at 573 K were investigated

Table 5
Estimated $(C_0 + \Delta C_0)/C_0$ and γ_s, $\Delta\gamma_s$, γ_s, $\Delta\gamma_p$ (J/m^2) for each RAF. (E = 200 GPa)

	F82H-IEA	F82H HT2	JLF-1	ORNL9Cr
$(C_0 + \Delta C_0)/C_0$	1.07	1.00	1.03	1.05
$\gamma_s + \gamma_p$	0.41	0.47	0.60	0.68
$\gamma_s + \Delta\gamma_s + \gamma_p + \Delta\gamma_p$	1.14	1.07	1.24	1.88
$\Delta\gamma_s + \Delta\gamma_p$	0.73	0.60	0.64	1.20

in this study. The following is a summary of the important conclusions:

1. Large ΔDBTT of irradiated F82H-IEA and F82H HT2 is the result of irradiation hardening.
2. Smaller ΔDBTT of irradiated JLF-1 is the result of smaller irradiation hardening at low temperature.
3. Small irradiation hardening of JLF-1 at low temperature could be the result of lath recovery during irradiation.
4. Smaller ΔDBTT of irradiated ORNL9Cr is the result of a large increase of fracture stress after irradiation.
5. The large increase of fracture stress is achieved by irradiation induced Ta resolution. This is indicated by XRD analysis on extracted precipitate residue that shows the dissolution of TaC (MX) precipitates.

Acknowledgements

The authors would like to thank Mr J.L. Bailey and J.W. Jones for their help on establishing the procedure for making extraction residue, and to Dr E.A. Payzant for carrying out XRD analysis. This research was sponsored by the Japan Atomic Energy Research Institute and the Office of Fusion Energy Sciences, US Department of Energy under contract DE-ACO5-00OR22725 with UT-Battelle.

References

[1] K. Shiba, M. Suzuki, A. Hishinuma, J. Nucl. Mater. 233–237 (1996) 309.
[2] K. Shiba, A. Hishinuma, J. Nucl. Mater. 283–287 (2000) 474.
[3] H. Tanigawa, M.A. Sokolov, K. Shiba, R.L. Klueh, Fusion Sci. Technol. 44 (2003) 206.
[4] H. Tanigawa, H. Sakasegawa, S.J. Zinkle, R.L. Klueh, A. Kohyama, DOE/ER-0313/35 (2003) 30.
[5] H. Tanigawa, H. Sakasegawa, E.A. Payzant, S.J. Zinkle, R.L. Klueh, A. Kohyama, DOE/ER-0313/35 (2003) 37.
[6] N. Hashimoto, H. Tanigawa, K. Shiba, R.L. Klueh, DOE/ER-0313/35 (2002) 24.
[7] N. Hashimoto, H. Tanigawa, M. Ando, T. Sawai, K. Shiba, R.L. Klueh, DOE/ER-0313/35 (2003) 41.
[8] Y. Kohno, A. Kohyama, M. Yoshino, K. Asakura, J. Nucl. Mater. 212–215 (1994) 707.
[9] H. Tanigawa, M. Ando, Y. Katoh, T. Hirose, H. Sakasegawa, S. Jitsukawa, A. Kohyama, T. Iwai, J. Nucl. Mater. 297 (2001) 279.
[10] T.L. Anderson, Fracture Mechanics: Fundamentals and Applications, 2nd Ed., CRC Press LLC, 1995, p. 285.
[11] R.L. Klueh, D.J. Alexander, M. Rieth, J. Nucl. Mater. 273 (1999) 146.
[12] H. Sakasegawa, M. Ando, H.Tanigawa, et al., Reported at Japan Inst. of Metal, Fall meeting, Fukuoka, Japan, 2001.
[13] M. Tamura, K. Shinozuka, K. Masamura, K. Ishikawa, S. Sugimoto, J. Nucl. Mater. 258–263 (1998) 1158.
[14] K. Shiba, M. Enoeda, S. Jitsukawa, in these Proceedings.